CCFE
CULHAM CENTRE FOR FUSION ENERGY

UK Atomic Energy Authority

UKAEA-CCFE-PR(25)331

K. Lee, L. Casali, J. Smiskey, D. Moulton, P. Ryan, N. Lonigro

The Effects of Gas Puff Locations and Divertor Closure on Detachment Conditions in MAST-U

The Effects of Gas Puff Locations and Divertor Closure on Detachment Conditions in MAST-U

K. Lee, L. Casali, J. Smiskey, D. Moulton, P. Ryan, N. Lonigro

This is a preprint of a paper submitted for publication in
Nuclear Fusion

The Effects of Gas Puff Locations and Divertor Closure on Detachment Conditions in MAST-U

K. Lee[1], L. Casali[1],J. Smiskey[1], D. Moulton[2], P. Ryan [2], N. Lonigro[3]

[1]University of Tennessee-Knoxville, Department of Nuclear Engineering
[2]UKAEA, Culham Science Centre, Abingdon, Oxfordshire, OX14 3DB, United Kingdom
[3] York Plasma Institute, University of York, United Kingdom

Abstract

The effect of different D_2 fueling locations and divertor closure in the MAST-U is studied in detail with the SOLPS-ITER code to gain insights to detachment physics in H-mode plasma experiments in conventional divertor (CD) configuration. The SOLPS-ITER simulations for MAST-U H-mode plasma reveals that changing D_2 fueling location significantly impacts the detachment condition. Under lower outer divertor (LOD) fueling, the total power loss at the lower outer divertor (LOD) is higher compared to the midplane fueling scenario for the same electron density at the outboard midplane side ($n_{e,sep}^{OMP}$). With LOD fueling in closed configuration, the analysis demonstrates substantial reductions on the peak heat flux and electron temperature at the lower outer divertor (LOD), facilitating the detachment onset due to an increased D neutral density and enhanced radiation, while suppressing carbon (C) sputtering. The closed divertor shows higher neutral trapping capability under both midplane and LD fueling. With LD fueling, the peak plasma temperature (T_e) show greater reduction in the closed divertor compared to the open divertor and the roll over of main ion flux (Γ_i) happens at $\sim$ 40% lower $n_{e,sep}^{OMP}$ in the closed divertor. These differences between divertor closure diminish when the midplane fueling is used. The analysis of all four scenarios (midplane/LD fueling in closed/open divertor) show that divertor closure and localized fueling work in synergy to create the optimized neutral trapping and energy dissipation, promoting detachment onset at lower $n_{e,sep}^{OMP}$. This work demonstrates that divertor closure and the localized fueling are both crucial to facilitate detachment onset at lower $n_{e,sep}^{OMP}$, highlighting the importance of an integrated approach to divertor optimization.

1. Introduction

A major challenge in the design and operation of future fusion machines lies in managing the power exhaust. For steady-state operation, the maximum heat flux to the target $q_{tg} \lesssim 10MW/m^2$ [1, 2, 3] and electron temperature at the target plate $T_e \leq 5eV$ [4] has to be satisfied. Exceeding these limits results in unacceptably high surface temperatures and material damage due to sputtering and melting [5], impacting the structural integrity of the wall material and potentially causing the eroded material to enter the plasma core and degrade the confinement [6, 7]. To guarantee the lifetime of the wall components and plasma performance, a robust power exhaust control is required.

In order to keep the heat load below the material limits, future fusion reactors are required to operate in the detachment regime [8], characterized by a cold dissipative divertor with high energy radiation losses from the SOL, low electron temperature near the divertor plates, and significant decrease of particle flux onto the targets [9]. Divertor detachment can be achieved by increasing upstream density through additional fueling to lower divertor electron temperature (T_e) [4]. Another common approach to access detachment is to introduce extrinsic impurities at the plasma edge to cool the plasma [10, 11, 12], which can provide access to detachment with lower upstream density. It has been shown in studies on tokamaks [13, 14, 15] that increasing upstream density through gas fueling might lead to degradation in confinement. To improve the compatibility between detachment and core confinement, a strategy that facilitates detachment onset with lower upstream density is required. Previous studies [16, 17, 18, 19] have shown that higher divertor closure can improve neutral trapping, enhancing the interactions between plasma and neutral particles by increasing the neutral density, which leads to greater momentum loss and reduction in particle flux to the target. While an open divertor allows neutrals to scatter more freely into the scrape-off layer (SOL), a closed divertor effectively confines neutrals within the divertor region [20, 21].

In this study, we present one of the first SOLPS modeling for MAST-U H-mode plasma. MAST-U offers a versatile range of in divertor configurations. Some of the examples include: short-leg conventional divertor (CD), elongated divertor, and the super-X divertor [22, 23]. Here a double null topology in the conventional divertor (CD) configuration is explored. By leveraging SOLPS-ITER's ability to model neutral distribution self-consistently, this study aims to elucidate how the fueling location affects the power asymmetry at the target. In addition to the effects of changing the deuterium (D) fueling location, the influence of divertor configurations (open vs closed)

on neutral baffling and detachment conditions was also examined.

The paper is organized as follows. In section 2, we present an overview of the reference H-mode plasma discharge used for this work. The SOLPS modeling inputs are described in section 3. In section 4, we compare the data obtained from the experiment (discharge #49392) to the SOLPS values, ensuring that the midplane and target profiles from SOLPS simulation agree with the experimental data. Additionally, we compare the 2D profiles of D_α and CIII reconstructed with multi-wavelength imaging (MWI) diagnostic system and the synthetic diagnostic for SOLPS. The results from the fueling location scan and divertor configurations comparisons are presented in section 4.1 and 4.2 respectively. Finally, the summary and discussion are given in section 5.

2. Experiment Overview

The SOLPS modeling presented in this work is set up in an interpretive manner based on a MAST-U double-null H-mode plasma with plasma current I_p = 0.75 MA, toroidal field on axis B_0=0.55 T, neutral beam injection power P_{NBI} = 3.3 MW, with the major and minor radii R=1 m and a=0.55 m respectively. The magnetic equilibrium is shown in Fig.1e. Time traces of the reference scenario are shown in Fig. 1 (a-d). The auxiliary heating is provided by two neutral beams (SS and SW). The power injection from the two beams is 1.6 MW and 1.7 MW respectively (Fig. 1a). The D_α signal is plotted in Fig. 1b to show the ELM activities during the discharge. The separation between primary and secondary separatrices mapped to the outer midplane (OMP), δr_{sep}, is shown in Fig. 1c; positive values correspond to an upper primary X-point, which suggests that the power flux can be biased toward the upper divertor [24]. The D_2 fueling is injected through the high-field side (HFS) midplane valve. The gas flux shown in Fig. 1d is the D_2 fueling flow rate [molecules s^{-1}] during the experiment. A more detailed description and analysis on this experiment can be found in [25].

3. SOLPS Modeling Inputs

The modeling results presented in this paper were obtained with the SOLPS-ITER code package (version 3.0.8), which consists of the multi-fluid plasma transport code B2.5 [26] for electrons and ions at each ionization state, coupled to the kinetic Monte Carlo code EIRENE for neutrals [27]. Both deuterium plasma species and carbon impurities (D and C) are considered in the calculations. Electrons and ions transport is treated by the fluid code, which provides the background plasma on which the neutral trajectories and particle sources are computed by EIRENE. EIRENE takes into account detailed atomic processes such as ionization, volume recombination, charge exchange, and elastic collisions [28, 29].

In this work, we present simulations of two divertor configurations: closed (Fig. 2a) and open (Fig. 2b). The computational grid for the closed divertor configuration (Fig. 2a) is obtained using the magnetic equilibrium from the plasma discharge number #49392 in MAST-U at 0.5 s, which corresponds to the double-null topology. The grid for the open divertor configuration (Fig. 2b) was generated using the Tokamak Exhaust Designer (TED) [30] based on the magnetic equilibrium for the closed divertor configuration where the outer strike point is shifted toward the high field side by 20 cm, increasing the distance between the plasma and the nose baffle. The plasma grid has a poloidal resolution of $R = 146$ cells and a radial resolution of $Z = 38$ cells. The same resolution is used for the generation of both closed and open divertor meshes. The total input power flowing from the core boundary, P_{SOL} = 1.6 MW, is divided equally between ions and electrons. The input power is not set according to the injected power of the reference experimental scenario because not all NBI power is absorbed and some of the power is lost through fast ions [31, 32]. Instead, P_{SOL} is set to match the electron temperature in the core measured by the Thomson scattering.

As stated above, two fueling scenarios for D_2 are simulated: one at the inner midplane, corresponding to the real fueling location in the experiment, and the other one at the lower outer divertor (LD) as shown in Figure 2. In order to carry out a systematic scan of plasma density, the fueling gas injection rate of D_2 is varied from 3×10^{21} nucleis s^{-1} to 1×10^{23} nucleis s^{-1}. The cross-field transport coefficients are anomalous and set to match the midplane profiles obtained from an H-mode MAST-U plasma (discharge #49392) via the Thomson scattering data obtained at 0.5s of the plasma discharge. The radial variation of the diffusion coefficients is plotted in Fig. 3. It has to be pointed out that the anomalous transport coefficients at the lower and upper outer PFR are reduced by a factor of 20 compared to SOL and inner PFR values to better match the j_{sat} profiles observed in the experiment [33].

Since all the PFCs are made of carbon, the surface reflection models were adopted from a TRIM database [34] for D-C and C-C interactions. The physical sputtering yield of C is calculated via the modified Roth–Bohdansky formula [35], while chemical sputtering is calculated using the flux-dependent

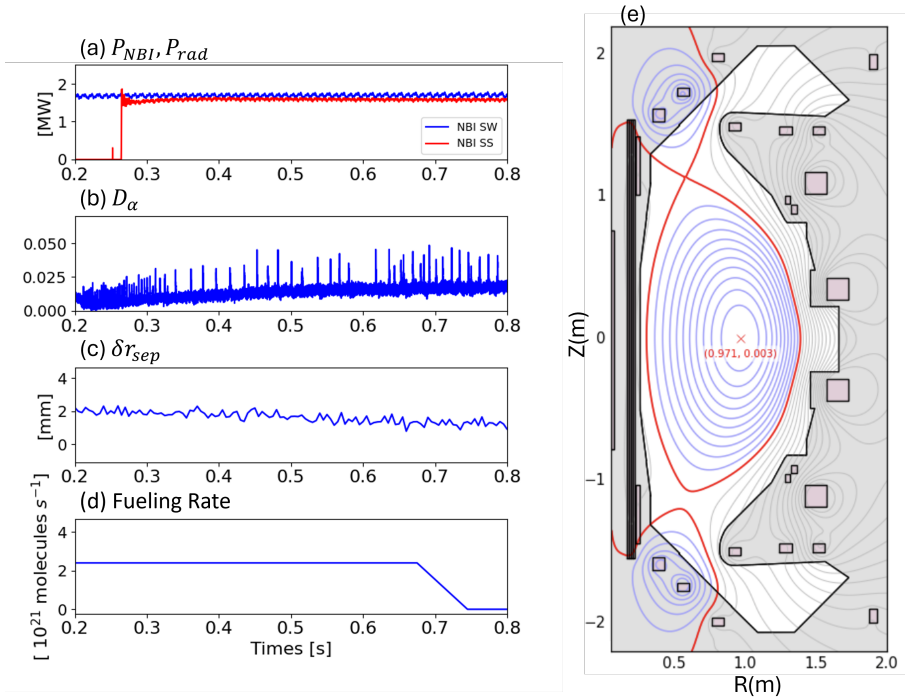

Figure 1: *Time traces of P_{NBI} and P_{rad} (a), D_α (b), δr_{sep} (c), D_2 fueling rate (d), and magnetic equilibrium (e) for the reference H-mode scenario (#49392).*

expression described in Roth's [36]. To reflect the fact that the target and the wall are not fully saturated with deuterium in the experiment, a small fraction of incident particles, corresponding to a wall absorption rate of $A_{wall} = 0.01$ %, was absorbed for all D and C species (ions, atoms and molecules)[37, 33]. Two pumping locations were placed at upper and lower divertor (Fig. 2), each with an absorption rate of $A_{pump} = 2.88\%$, equivalent to a pumping speed of approximately 10 m^{-3} s^{-1}.

At the target, the standard Bohm-Chodura sheath condition described in Section 4 of Dekeyser's [38] is applied. Leakage-type boundary conditions are used at the far scrape-off layer (SOL) and in the private flux region (PFR), where radial particle, electron, and ion heat flux densities are set to factors of 10^{-2},10^{-4}, and 2×10^{-2}, of the local sound speed. To capture kinetic effects below the formal validity range of fluid equations, parallel flux limiters were implemented using the harmonically averaged formulation described in [39]. The electron and ion parallel flux limiters are set to α_{χ_e}=0.3 and α_{χ_i}=1.0 respectively, with the ion parallel viscous flux limiter set to α_{η_i}=0.5. As this work represents the initial stage of SOLPS modeling of an H-mode plasma discharge in MAST-U, drift effects were not included. Further efforts will focus on incorporating drift physics and validating the results to this work. The simulation setup described above, except for equilibrium, fueling locations, and transport coefficients, is taken from [33].

4. SOLPS Results and Comparisons to Experimental Data

The cross-field transport coefficients (D and χ) for the simulations (shown in Fig. 3) are set to match the experimental profiles. Fig. 4 shows the comparison of midplane n_e and T_e profiles between the experimental data and simulation results with an overall good match. The scattered points are Thomson scattering [40] data obtained within a 50 ms window (0.5-0.55 s) of the plasma discharge, while the red curve represents the profiles from the simulation. Fig. 5 showcase the comparison of the ion saturation current density (J_{sat}), parallel heat flux ($q_\parallel$), T_e, and n_e profiles at the outer lower target between the Langmuir probe [41] measurement and the simulation. The $q_\parallel$ and n_e profiles in the simulation match well to the Langmuir probe measurement, the peak value of J_{sat} and T_e profiles in the simulation are instead overestimated and underestimated by 25% and 30% respectively compared to the Langmuir probe measurement. This discrepancy could be caused by the fact that the electron temperature measurement is sensitive to only the tail of the electron energy distribution function (EEDF), so the measurement would not be representative of the overall distribution, but rather the hot population in the case of a non-Maxwellian EEDF. The specific SOLPS case we use for these comparisons is the inner midplane fu-

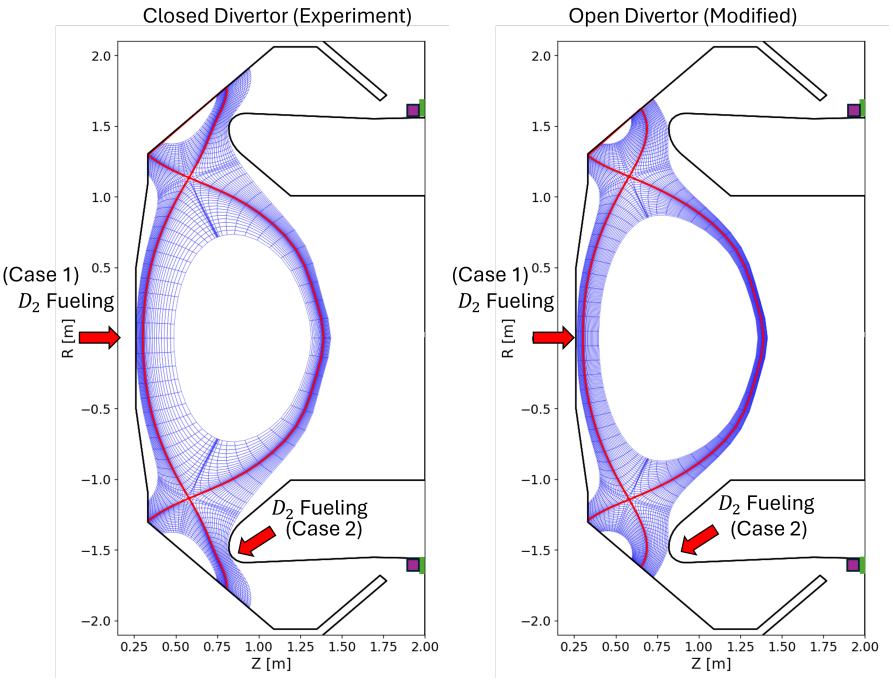

Figure 2: *Computational grid established with the magnetic equilibrium from MASTU discharge #49392 (left) and the grid established with modified magnetic equilibrium (right). Two different fueling locations (inner midplane and lower divertor) were set for two scenarios. The fueling location for midplane fueling scenario (case 1) is the same location used in the experiment and is set at (R,Z)=(0.260,0)[m] while the location for LD fueling scenario (case 2) is at (R,Z)=(0.822,-1.5)[m]. Two pump locations were set at the upper and lower divertor respectively (green area). The purple areas mark the locations of the neutral pressure gauge.*

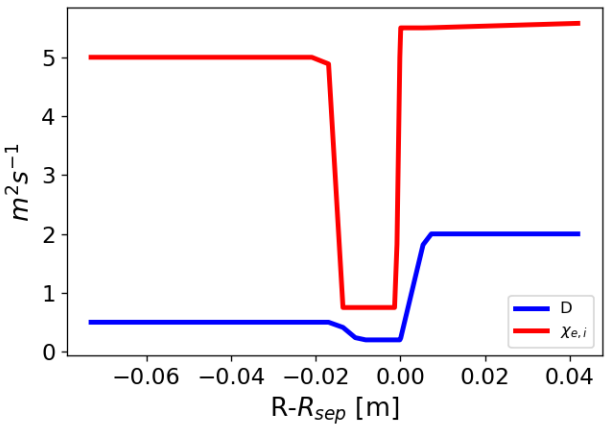

Figure 3: *The cross-field anomalous diffusion transport coefficients (D) and heat conductivities ($\chi_{e,i}$), both in m^2s^{-1}, along the outer midplane. The x-axis is the distance from the separatrix at the outer midplane in m.*

eling scenario in closed divertor geometry with D_2 fueling rate of 5×10^{21} molecules s^{-1}, which is 2.5 times higher than the puffing rate in the experiment (2×10^{21} molecules s^{-1}).

MAST-U is equipped with a multi-wavelength imaging (MWI) filtered camera diagnostic system [42, 43]. Figure 6 shows 2D MWI reconstruction of the D_α emissivity in the poloidal plane for plasma discharge #49392 (a) and the SOLPS simulation (b). It is observed that the D_α emission from the SOLPS simulation agrees with the experimental profile qualitatively throughout the divertor leg except for the area near the target where SOLPS predicts around 2 times higher emissivity compared to the experimental measurement. The MWI system is also equipped with filters for C_{III} emissivity. However, the coverage for C_{III} emission is limited to only part of the conventional divertor region. (Fig. 7). As shown in Fig. 7, SOLPS predicts at least an order of magnitude lower CIII emission at the target compared to the experimental data for MWI, which could be attributed to high sputtering during the plasma discharge in the experiment.

Another important quantity for the divertor study is the neutral pressure. We compare the neutral pressure at the divertors from the simulation to the experimental measurements from the neutral pressure gauges (Fig. 8). The locations of the gauges are

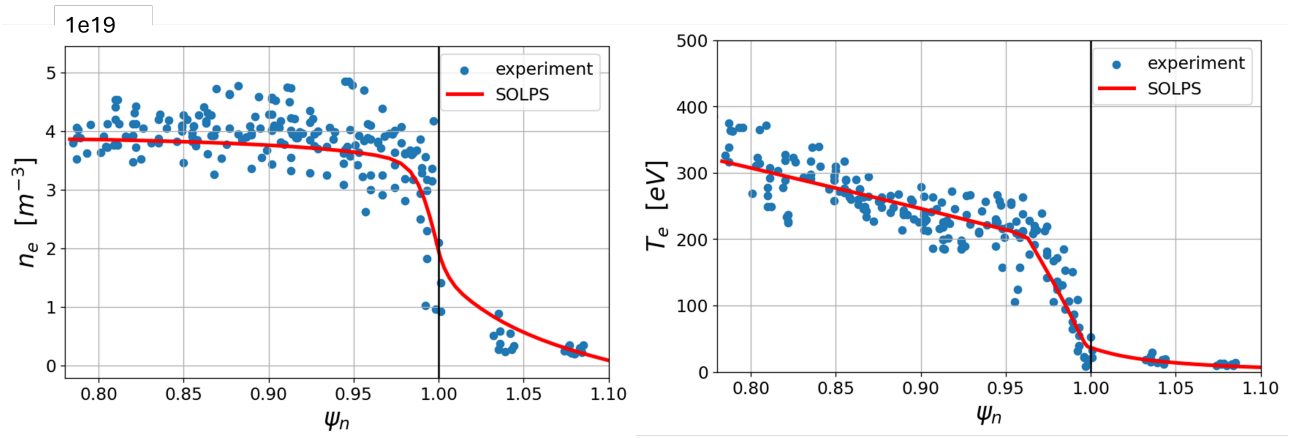

Figure 4: *Midplane profiles of (a) Electron density (n_e) and (b) electron temperature (T_e) from the experiment (blue dots) and SOLPS simulation (red curve) at the outer midplane. The x-axis is the normalized magnetic axis (ψ_n), where the separatrix (marked by the black line) is located at $\psi_n = 1$. The SOLPS simulation selected for the comparison is inner midplane fueling with a rate of 1×10^{22} $\frac{atoms}{s}$ in closed divertor geometry.*

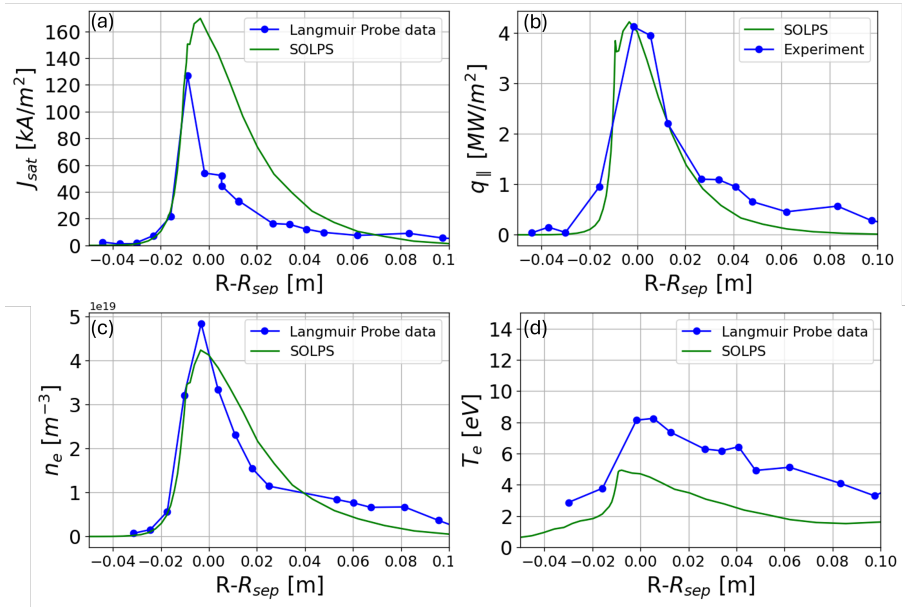

Figure 5: *The (a) Ion saturation current density J_{sat}, (b) Parallel heat flux $q_{\parallel}$, (c) Electron density n_e, and (d) electron temperature T_e radial profiles at the outer lower target from the Langmuir probe measurements (blue dots) and SOLPS-ITER simulation (green curve). All the profiles are plotted as a function of major radial distance past the separatrix.*

marked by the purple area in Fig. 2. In Fig. 8, we observe that the neutral pressure at both upper and lower divertors from SOLPS simulation closely matches the measurements from the experiment at the upper divertor neutral pressure gauge at 0.5 s of the discharge. The neutral pressure measurement from the lower divertor is lower by $\sim 25\%$ compared to the upper divertor throughout most of the discharge. This may be caused by the combination of asymmetry in the magnetic equilibrium and drift effects [24].

4.1 Effects of Fueling Locations in a Closed Divertor

The location of deuterium fueling can play a critical role in determining divertor conditions, which may have an impact on the particle transport and the neutral recycling. The following results examine the impact of different gas puff locations in a closed divertor. Two different fueling locations are used: one located at the inner midplane, corresponding to the experiment, with coordinates of (R,Z)=(0.26,0.00) and LD where the valve is set at (R,Z)=(0.82,-1.50). It has to be pointed out that the actual gas valve used in the experiment is slightly above the midplane (Z = 0.2m), but such a small difference does not carry

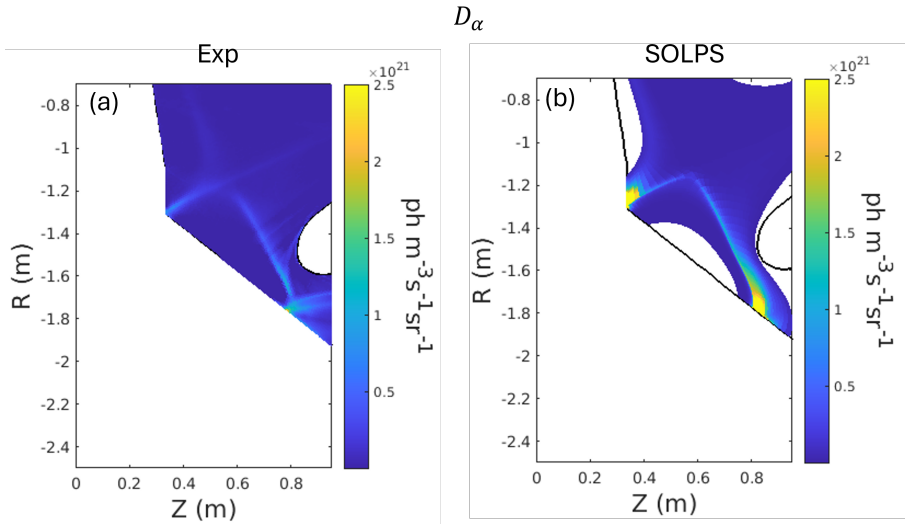

Figure 6: *D_α emissivity obtained from MAST-U MWI system at 0.5s of the discharge* #49392 *(a) and reconstructed by synthetic diagnostic for SOLPS (b)*

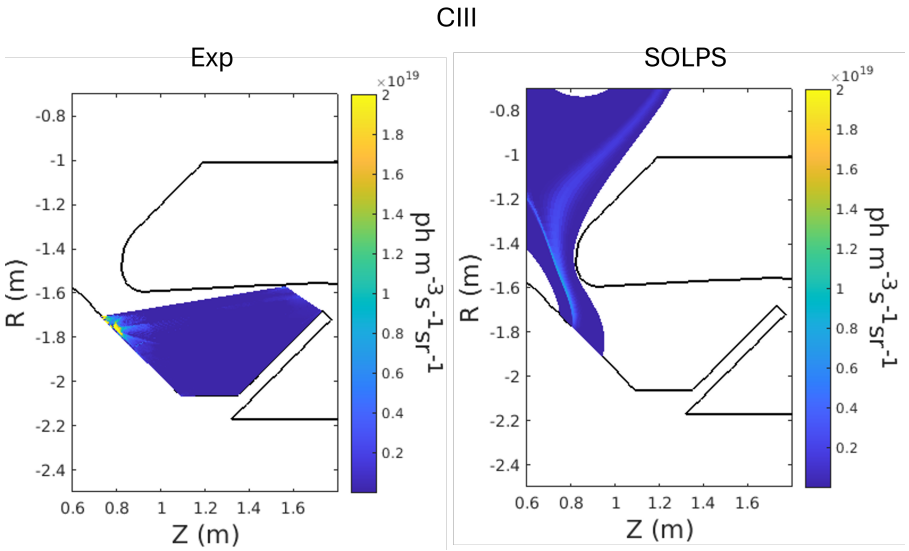

Figure 7: *C_{III} emissivity obtained from MAST-U MWI system at 0.5s of the discharge* #49392 *(a) and reconstructed by synthetic diagnostic for SOLPS (b)*

significance in SOLPS-ITER simulations. For the following discussion, we will focus on the conditions at the LOD, as it will likely be affected by the change of fueling location the most. To understand the effects of fueling location on power dissipation, we evaluate the total power loss (Fig. 9) and the radiation loss from D and C (Fig. 10) at the lower outer divertor (LOD) as a function of $n_{e,sep}^{OMP}$. In these figures, the square markers represent SOLPS-ITER simulations with different fueling rates and their corresponding upstream density ($n_{e,sep}^{OMP}$) is calculated and used as the x values. Under the same fueling rates, the $n_{e,sep}^{OMP}$ values for midplane and LD fueling scenarios are very different. For example, the $n_{e,sep}^{OMP}$ for midplane fueling and LD fueling under 1×10^{23} nucleis s^{-1} are $6.3 \times 10^{19} m^{-3}$ and $2.2 \times 10^{19} m^{-3}$ respectively (Fig. 9), suggesting that the increase in upstream density under LD fueling is not as sensitive to fueling compared to midplane fueling. As shown in Fig. 9, the total power loss at the LOD under LD fueling is consistently higher throughout the scans. More specifically, the D radiation loss at LOD under the LD fueling is higher compared to the midplane fueling. In terms of radiation losses, the C radiation loss under midplane and LD fueling scenarios is at least an order of magnitude lower compared to the D radiation losses, which indicates that D radiation is the dominant energy loss mechanism. To examine the distribution of the radiation loss in the divertor regions, we evaluate the 2D distribution of D (Fig. 11) and C (Fig. 12) radiation in the divertor regions. Fig. 11 and Fig. 12 show the 2D maps of the D and C radiation at

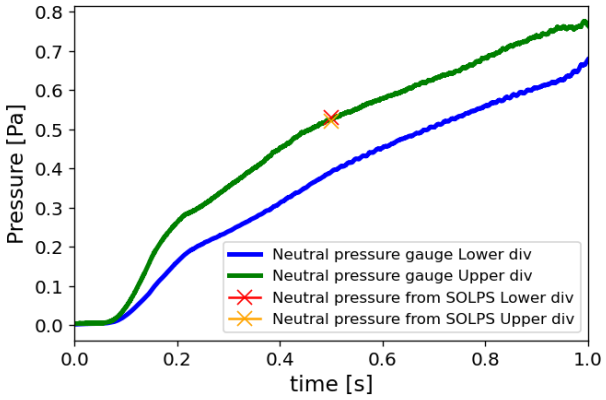

Figure 8: *Neutral pressure measurements from pressure gauge at upper divertor (green) and lower divertor (blue) during discharge 49392. The cross marker represents the neutral pressure value calculated by SOLPS (orange) and lower divertor (red).*

the upper and lower divertor, comparing the two fueling scenarios for a closed divertor configuration with $n_{e,sep}^{OMP} = 1.25 \times 10^{19} m^{-3}$. In both cases, the D radiation at the lower outer divertor (LOD) region is higher than the C radiation by two orders of magnitude. In the SOLPS-ITER simulations, the C radiation at the LOD under LD fueling is 87 % lower compared to the midplane fueling scenario. The D radiation under LD fueling is 8 % higher compared to midplane fueling in that region. The slightly higher D radiation at LOD under the LD fueling scenario may be attributed to the higher neutral D density in that region while the weaker C radiation can be associated with lower C density. This can be demonstrated by looking at the 2D neutral density distribution for D and C (n_D and n_C), plotted in (Fig. 13 and Fig. 14), where n_D at the LOD is found to increase under the LD fueling while n_C is found to decrease. However, the reduction in n_C may not be the only factor impacting the low C radiation in that region. The strength of the C radiation is also affected by the conditions of the plasma background (n_e and T_e). In the LD fueling case shown in Fig. 12, the average T_e at the upper outer divertor (UOD) is 8 eV while the average temperature at LOD is 4 eV. In this temperature range, C radiates more efficiently at the upper divertor [44]. To assess this in detail, we evaluate the C radiation with the expression below:

$$P_{rad} = n_e n_z L_z(T_e, n_e \tau_i) \quad (1)$$

Where n_e is the electron density, n_z is the impurity density, and L_z is the impurity radiation coefficient in non-coronal equilibrium which depends on temperature and the residence parameter $n_e\ \tau_i$, where τ_i is the residence time of the impurity [16, 45]. To test whether n_C is the most dominant factor, we flip the plasma parameters (n_e, T_e) and (n_C), in turn, from the final plasma state in the simulation between upper divertor and lower divertor and recalculate the C radiation with SOLPS-ITER by running a single time step of simulation after the flipping. By doing so, SOLPS-ITER will re-calculate the C radiation based on the altered plasma background (n_e,T_e) and impurity distribution (n_C). Since the C radiation at the upper divertor is stronger compared to the lower divertor, flipping the plasma background and impurity content between the upper and lower divertor will lead to the increase in C radiation at the lower divertor. The parameters that have the greatest impact on C radiation will result in a greater change in radiation after flipping the parameters. As illustrated by Fig. 15, when flipping n_e and T_e, C radiation at LOD increased by ~ 1.5 times. If only the n_C is flipped, the C radiation at the lower divertor increased by more than 3 times compared to the initial value before flipping. This result suggests that n_C is the main factor causing the low C radiation while n_e and $L_Z(T_e, n_e\tau_i)$ have weaker effects in comparison.

As previously discussed the low C radiation at LOD under LD fueling might be attributed to the reduced n_C relative to the upper divertor. One possible cause for the reduction in n_C at LOD under LD fueling is the suppressed C sputtering [46]. When T_e is significantly reduced ($T_e < 5eV$), the physical and chemical sputtering of C from the wall is suppressed [47]. To verify that the reduction in C sputtering plays a significant role in the reduction of n_C, we analyze the total flux of C sputtered from the wall at the LOD region under midplane and LD fueling across various $n_{e,sep}^{OMP}$. As shown in Fig. 16, total C sputtering at the LOD decreases significantly under LD fueling compared to midplane fueling. The underlying mechanisms driving this behavior can be attributed to a sequence of effects: first, the increased n_D in the lower divertor increases D radiation, leading to a reduction in local T_e. This T_e drop suppresses C sputtering, which in turn reduces the overall n_C. The reduced n_C ultimately results in weaker C radiation.

To understand how fueling locations affect detachment conditions, we evaluate important detachment sensitive parameters like heat flux ($q_\perp$) and T_e at the target for both midplane and LD fueling cases. The results of this investigation are plotted in Fig. 17. Here we use T_e as the main parameter with detachment occurring at T_e peak $< 5eV$. Fig. 17 shows the scan of different D_2 fueling rates for midplane and LD fueling. In both fueling scenarios, increasing the fueling rate led to reductions in $q_\perp$ and T_e peak at both upper and lower divertors. The $q_\perp$ peak at the upper divertor under the LD fueling scenario is higher compared to the midplane fueling

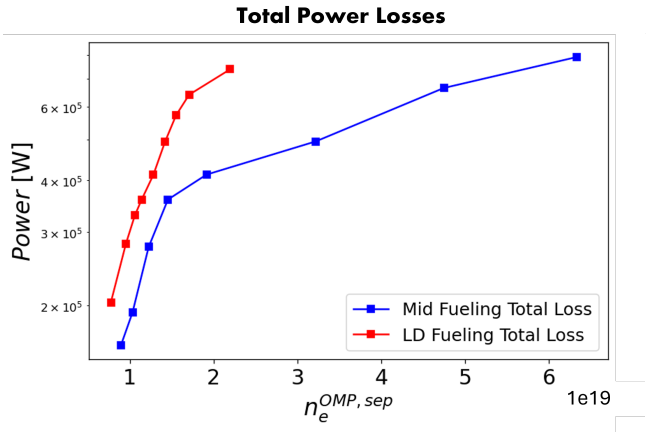

Figure 9: *Total power loss at the LOD under midplane fueling (blue) and LD fueling (red) scenario in closed divertor)*

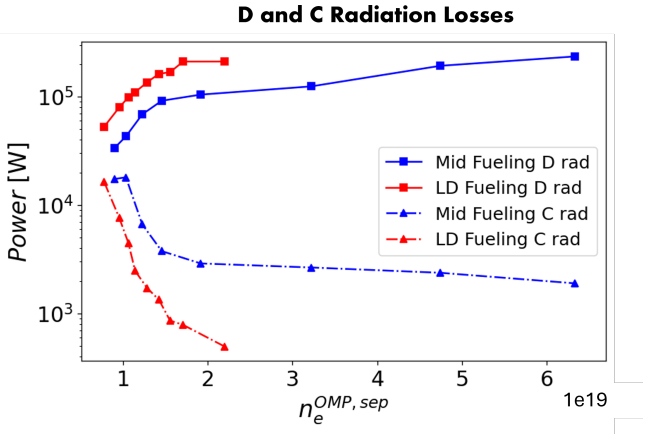

Figure 10: *D and C radiation loss at the LOD under midplane fueling (blue) and LD fueling (red) scenario in closed divertor*

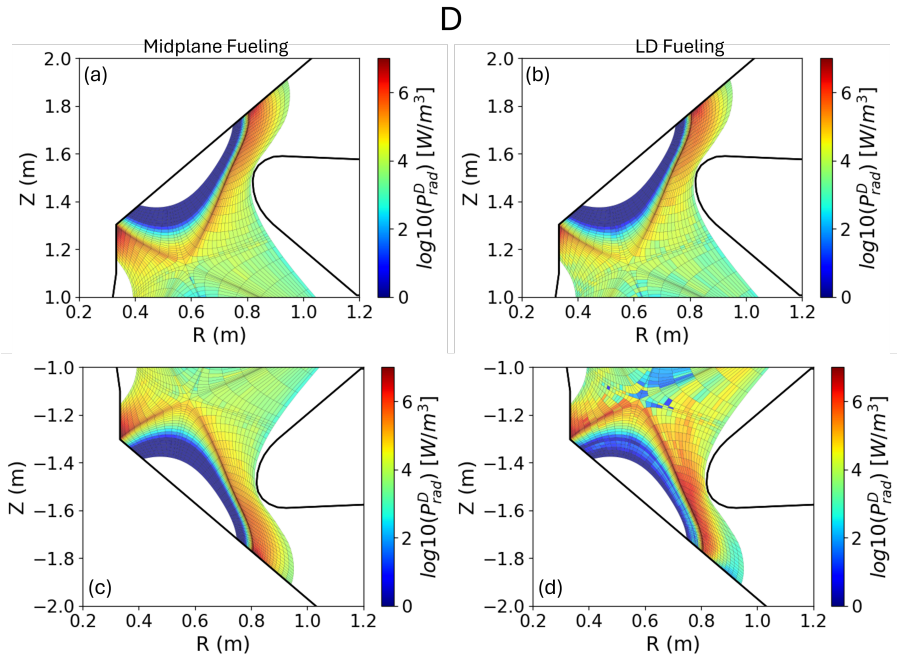

Figure 11: *2D distribution of D radiation at upper (a,b) and lower (c,d) divertors under midplane fueling (a,c) and LD fueling (b,d) scenarios with* $n_{e,sep}^{OMP} = 1.25 \times 10^{19}\ m^{-3}$

scenario across all fueling rates. The $q_\perp$ reduction at the lower divertor is much greater under the LD fueling scenario. At $n_{e,sep}^{OMP} = 1.25 \times 10^{19} m^{-3}$, the $q_\perp$ reduction under LD fueling scenario is about 89% more compared to the midplane fueling. Additionally, the T_e reduction at the lower divertor under the LD fueling scenario is about 82% more compared to the midplane fueling scenario. As illustrated in Fig. 17(d), the detachment at the outer lower divertor is achieved with 50 % lower $n_{e,sep}^{OMP}$ under LD fueling. The lowered threshold of detachment under LD fueling is due to the fact that the fueling location is much closer to the target, which increases n_D at the divertor (Fig. 13 d) and promotes higher energy dissipation through radiation and ion-neutral collisions [9]. The peak $q_\parallel$ and T_e at upper and lower outer targets under midplane fueling are almost identical (Fig. 17), which can be attributed to the top down symmetry of the geometry and model equations (in the absence of drifts). Under LD fueling, on the other hand, the peak $q_\parallel$ and T_e are higher at the upper outer target compared to the lower outer target (Fig. 17). This may be caused by the greater distance between the upper divertor and the fueling. When LD fueling is used, the upper target receives higher heat flux and is hotter compared to midplane fueling under similar upstream density (Fig. 17 a and c). The detachment onset at the upper divertor occurs earlier under mid-

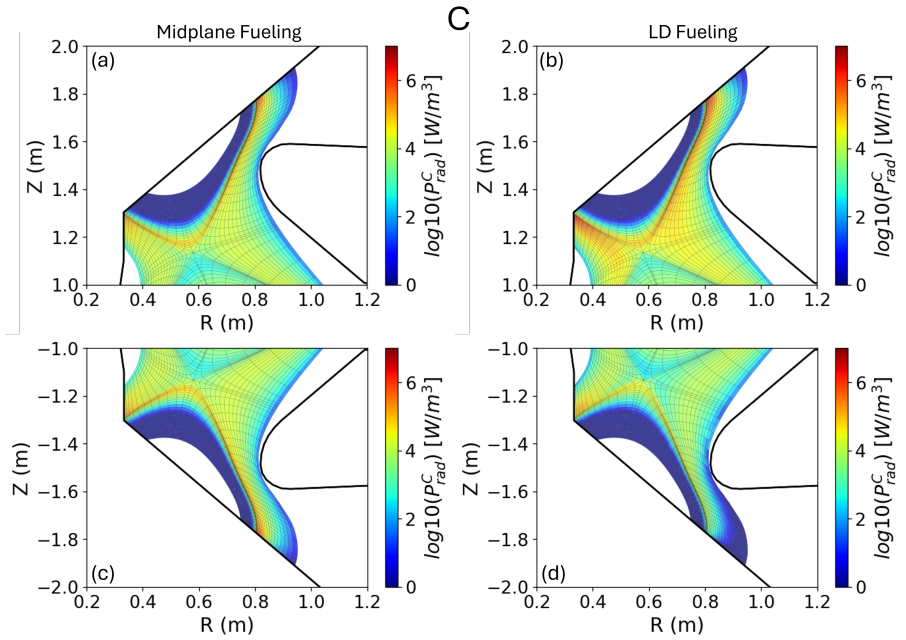

Figure 12: *2D distribution of C radiation at upper (a,b) and lower (c,d) divertors under midplane fueling (a,c) and LD fueling (b,d) scenarios with* $n_{e,sep}^{OMP} = 1.25 \times 10^{19}\ m^{-3}$.

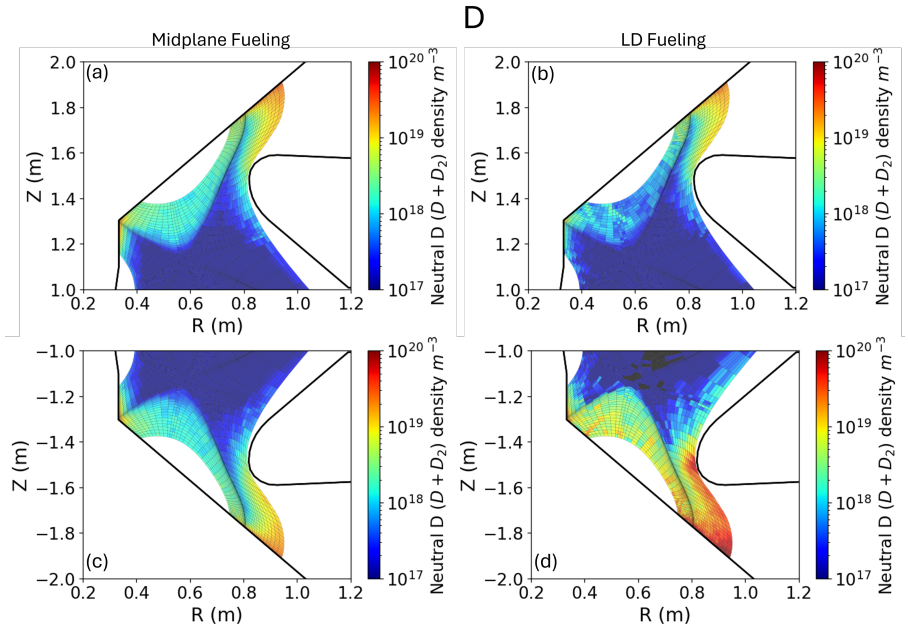

Figure 13: *2D distribution of D density at upper (a,b) and lower (c,d) divertors under midplane fueling (a,c) and LD fueling (b,d) scenarios with* $n_{e,sep}^{OMP} = 1.25 \times 10^{19}\ m^{-3}$.

plane fueling at $n_{e,sep}^{OMP} = 2 \times 10^{19} m^{-3}$ while it occurs at $n_{e,sep}^{OMP} = 3 \times 10^{19} m^{-3}$ under the LD fueling (Fig. 17 c). These observations have significant implications for the fueling strategy: The upper and lower divertor can be controlled independently with closed divertors, which is demonstrated in Kool's work [48]. In real-life cases where there are natural up-down asymmetries (e.g. due to drifts or imperfect double null), this is useful.

4.2 Effects of Divertor Closure on Detachment Conditions

In the previous discussion, we demonstrated that switching the D_2 fueling location from the inner midplane to the lower divertor in a closed divertor configuration results in a stronger reduction in both $q_\perp$ and

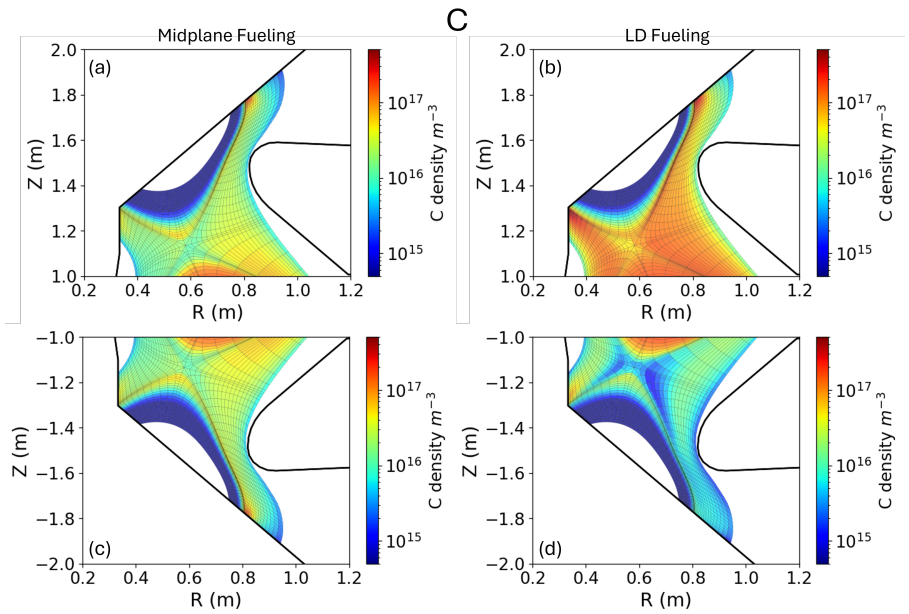

Figure 14: *2D distribution of C density at upper (a,b) and lower (c,d) divertors under midplane fueling (a,c) and LD fueling (b,d) scenarios with* $n_{e,sep}^{OMP} = 1.25 \times 10^{19}\ m^{-3}$.

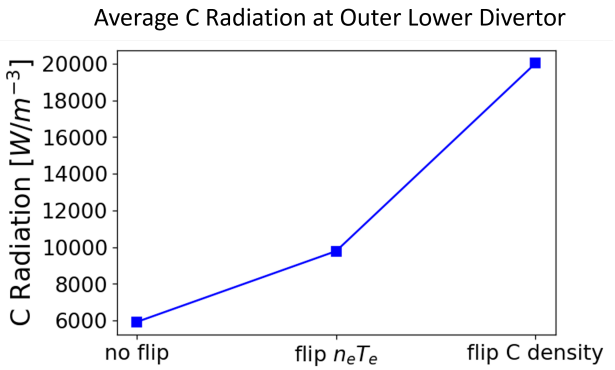

Figure 15: *Average C radiation at lower divertor calculated by SOLPS-ITER for LD fueling case with* $n_e^{OMP,sep} = 1.25 \times 10^{19} m^{-3}$. *The C radiation for three different cases is presented. C radiation before flipping the plasma state (no flip), C radiation after flipping* n_e *and* T_e *(flip* n_e T_e*), and C radiation after flipping C density (flip C density).*

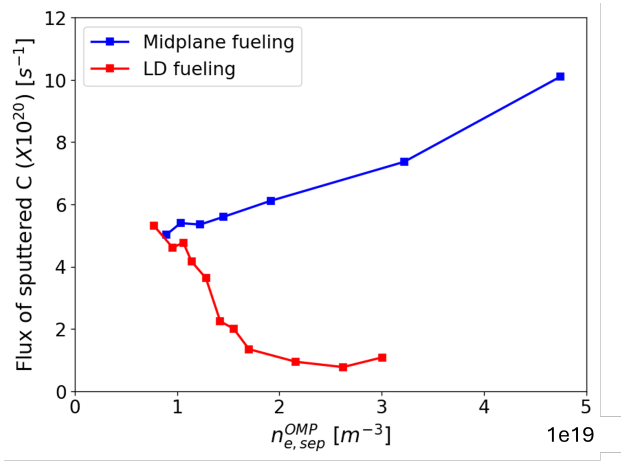

Figure 16: *Total C sputtering off the target wall at the outer lower divertor. LD fueling cases are represented by red lines and midplane fueling is represented by blue lines.*

T_e at the LOD. This reduction is attributed to the increased n_D in that region. To study the role of fueling locations on the divertor closure, we compare simulations in closed and open divertor configurations under both midplane and LOD fueling scenarios.

Fig. 18 shows the variation of T_e and Γ_i with $n_{e,sep}^{OMP}$ at the LOD for midplane fueling in both closed and open divertor configurations. Under midplane fueling, the closed divertor configuration does not yield a significant advantage in reducing T_e compared to the open configuration. Although the temperature reduction is more pronounced in the closed divertor at lower $n_{e,sep}^{OMP}$, the differences diminish as $n_{e,sep}^{OMP}$ increases. In the closed configuration, detach-

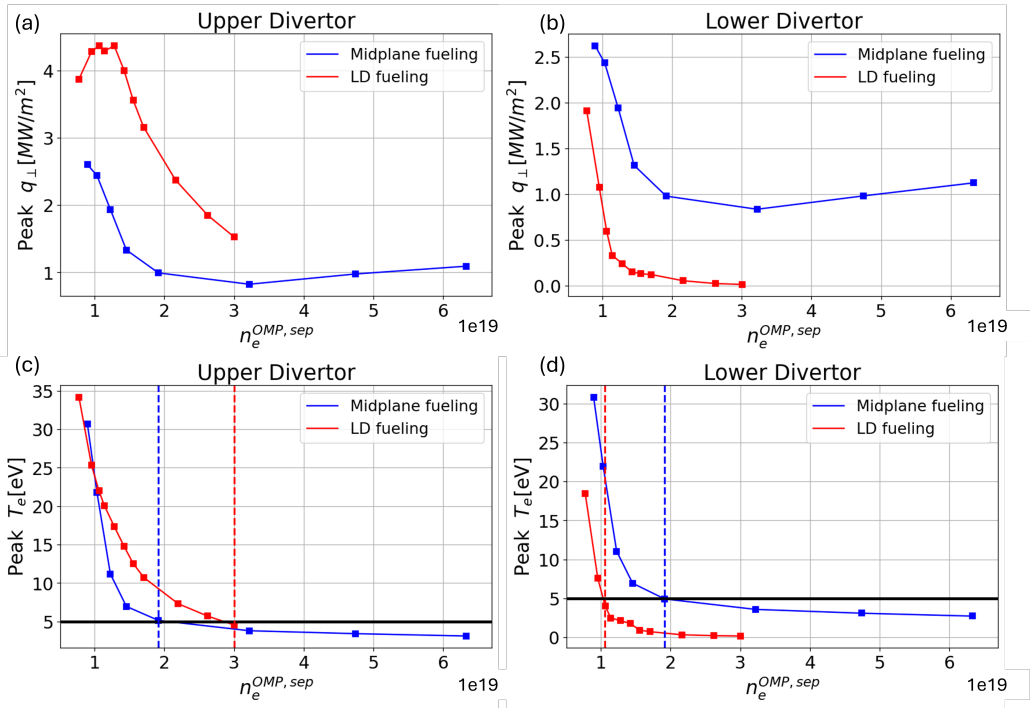

Figure 17: *Peak $q_\perp$ and T_e at lower and upper outer divertor targets with respect to $n_e^{OMP,sep}$. Values from midplane fueling cases are represented by blue lines while the LD fueling cases are illustrated by red lines. The onset of detachment at the divertors (upper and lower) under midplane and LD fueling scenarios are marked by the dashed lines.*

ment occurs at $n_{e,sep}^{OMP} = 1.9 \times 10^{19} m^{-3}$, differently at $n_{e,sep}^{OMP} = 2.1 \times 10^{19} m^{-3}$ in open configuration, accounting for 9.5% difference among the two. As illustrated by Fig. 18b, the Γ_i did not roll over in both closed and open configurations under midplane fueling. On the other hand, under the LD fueling scenario, the T_e at the outer lower target is consistently lower in closed divertor configurations at all range of $n_{e,sep}^{OMP}$. In the closed divertor configuration under LD fueling, the upstream density required to reach target temperature of 5 eV is $n_{e,sep}^{OMP} = 1.06 \times 10^{19} m^{-3}$ while it is $n_{e,sep}^{OMP} = 1.47 \times 10^{19} m^{-3}$ in the open configuration, which is $\sim$ 28% in difference (Fig. 19a). In both closed and open cases under LD fueling, the Γ_i to the target exhibits roll-over behaviors. In closed configuration, the roll-over happens at $n_{e,sep}^{OMP} = 1.7 \times 10^{19} m^{-3}$ while it occurs at $n_{e,sep}^{OMP} = 2.8 \times 10^{19} m^{-3}$ in the open configuration,which corresponds to $\sim$ 40% differences (Fig. 19b). The roll-over of Γ_i in both closed and open configurations under LD fueling suggests that a significant amount of neutral particles accumulate at the LOD, promoting more ion-neutral interactions which lead to greater momentum dissipation and reduction of Γ_i to the target [49]. These observation suggests that the divertor closure and localized fueling work in synergy to facilitate detachment onset with lower $n_{e,sep}^{OMP}$.

To provide quantitative analysis for the effects of fueling location and divertor configurations on neutral trapping, we evaluate the total neutral D particles (n_D^{tot}) at the LOD for all the four cases: closed and open divertor under midplane and LD fueling scanning various fueling rates (Fig. 20). The n_D^{tot} at the LOD is higher under the LD fueling compared to the midplane fueling scenario under the same fueling rates in the closed divertor configuration. The difference in n_D^{tot} between midplane and LD fueling rate grows larger as the fueling rate increases. The same trend is also observed when comparing midplane and LD fueling scenarios in open divertor geometry. When comparing between midplane and LD fueling scenario in closed configuration at 5×10^{22} nucleis s^{-1} fueling rate, the n_D^{tot} at the LOD under LD fueling is 220% higher than in the midplane fueling scenario —representing the largest observed difference among the comparison groups. In contrast, the neutral particle differences for other configuration pairs are notably smaller: 44% between closed and open divertors under midplane fueling, 89% between closed and open divertors under LD fueling, and 200% between LD and midplane fueling in the open configuration. From this observation, we conclude that the fueling locations have the most impact on the neutral contents at the LOD while the effects of closures are less pronounced.

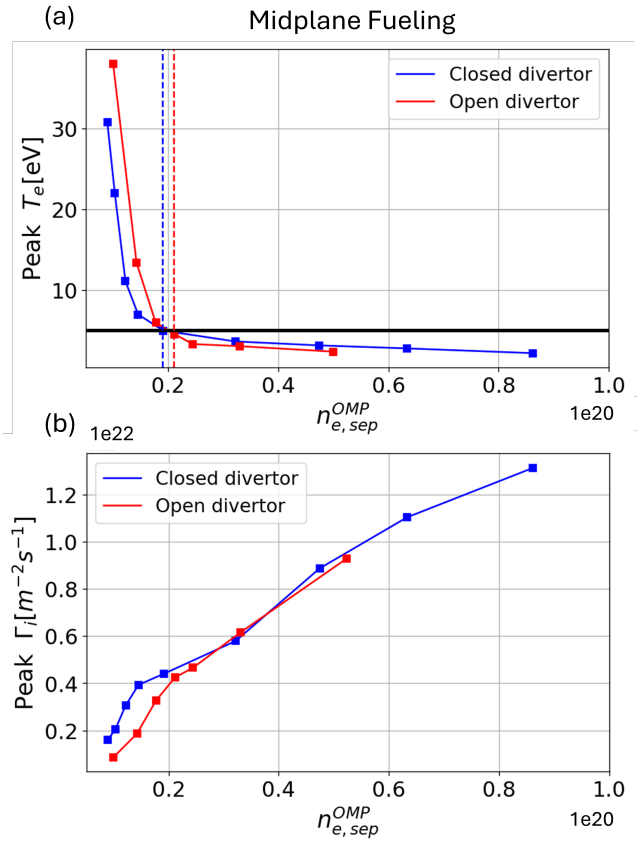

Figure 18: *Peak T_e (a) and Γ_i (b) at outer lower targets with respect to $n_{e,sep}^{OMP}$ under midplane fueling scenario. Values from the open divertor case are represented by red lines while the closed divertor case is indicated by blue lines.*

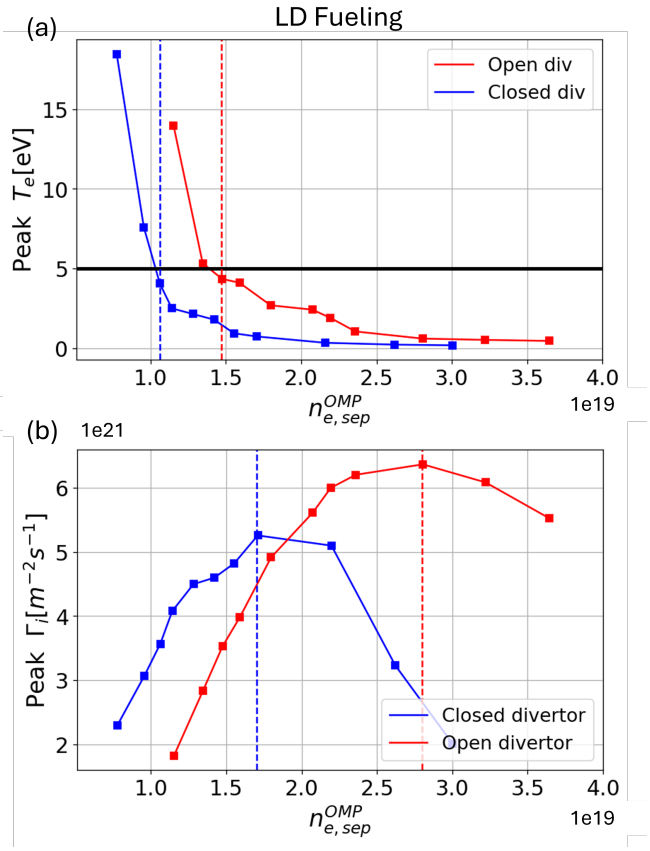

Figure 19: *Peak T_e (a) and Γ_i (b) at outer lower targets with respect to $n_{e,sep}^{OMP}$ under midplane fueling scenario. Values from the open divertor case are represented by red lines while the closed divertor case is indicated by blue lines.*

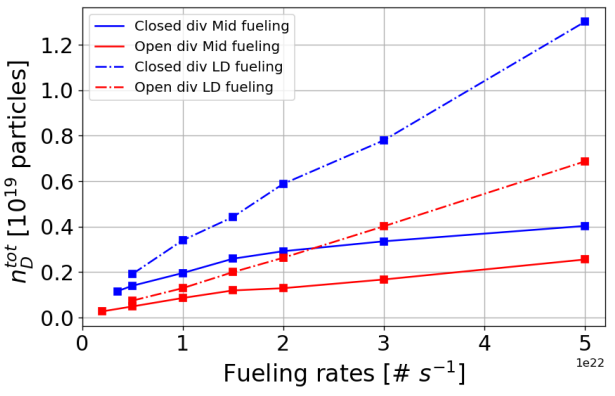

Figure 20: *Total neutral D contents (n_D^{tot}) at the LOD with respect to D_2 fueling rates. The closed divertor cases are represented by blue lines while the open cases are illustrated by the red lines. The solid lines represent the midplane fueling scenario and the dashed lines represent the LD fueling scenario.*

5. Conclusion

This study has systematically investigated the effects of D_2 fueling locations and divertor closure on divertor conditions in experiments performed at the Mega Ampere Spherical Tokamak Upgrade (MAST-U) using numerical modeling with SOLPS-ITER. The simulations are based on the experimental MAST-U H-mode plasma discharge (#49392) in the conventional divertor (CD) configuration. Midplane profiles from the SOLPS case with midplane fueling in a closed divertor geometry were matched to Thomson scattering [40] data. Additionally, simulated target profiles, neutral pressures, and emissivity profiles were compared with Langmuir probe [41] measurements, neutral pressure gauge data, and multi-wavelength imaging (MWI) spectroscopy [42].

The results show that fueling location significantly influences divertor behavior. Lower divertor (LD) fueling increases n_D in the LOD, enhancing radiation and promoting detachment onset at lower $n_{e,sep}^{OMP}$. This leads to a substantial reduction in peak heat flux $q_\perp$ and electron temperature T_e at the LOD. These observations are consistent with previous observations

made in [16, 20] for DIII-D tokamak. Furthermore, LD fueling reduces local T_e which suppresses carbon sputtering, thereby decreasing carbon radiation, while the overall radiation remains high due to the increased deuterium radiation. Under LD fueling in the closed divertor geometry, the peak $q_{\parallel}$ and T_e at the upper divertor remain relatively high due to its greater distance to the fueling location. This observation implies that a localized LD fueling can be employed to cool the lower divertor target without affecting the upper divertor significantly.

Under LD fueling, the closed divertor configuration consistently achieves lower $q_{\perp}$ peak and T_e across all the scanned fueling rates. Detachment onset occurs at a 28% lower $n_{e,sep}^{OMP}$ and the roll over of Γ_i occurs at 40% lower $n_{e,sep}^{OMP}$ compared to the open divertor, attributed to enhanced neutral trapping and increased radiative and collisional energy dissipation. In contrast, under midplane fueling, these effects are significantly diminished due to the greater distance between the fueling source and the divertor.

Evaluation of the total deuterium neutral content (n_D^{tot}) further supports these findings. At a fueling rate of 5×10^{22} nucleis $s^{-}1$, LD fueling with a closed divertor yields a 220% higher n_D^{tot} at LOD compared to midplane fueling in the same divertor configuration. Additional comparisons reveal consistent trends: a 44% increase between closed and open divertors under midplane fueling, an 89% increase between closed and open divertors under LD fueling, and 200% increase between LD and midplane fueling in the open configuration.

Overall, this comparative evaluation highlights the importance of an integrated approach to divertor optimization. While divertor closure and baffling improves neutral trapping, its effectiveness is significantly enhanced when combined with localized fueling. The combination of LD fueling and a closed divertor provides the most favorable conditions for achieving detachment at lower upstream densities, consisting in an essential requirement for balancing core confinement with power exhaust in future fusion devices.

Acknowledgments

This work is supported by US Department of Energy under DOE Grant DE-SC0023381 and Nuclear Regulatory Commission under NRC Grant # 31310022M0014 and

References

[1] AR Raffray et al. “High heat flux thermal–hydraulic analysis of ITER divertor and blanket systems”. In: *Fusion engineering and design* 39 (1998), pp. 323–331.

[2] Takeshi Hirai, Koichiro Ezato, and Patrick Majerus. “ITER relevant high heat flux testing on plasma facing surfaces”. In: *Materials Transactions* 46.3 (2005), pp. 412–424.

[3] James P Gunn et al. “Surface heat loads on the ITER divertor vertical targets”. In: *Nuclear Fusion* 57.4 (2017), p. 046025.

[4] Peter C Stangeby. *The plasma boundary of magnetic fusion devices*. CRC Press, 2000.

[5] VP Budaev. “Results of high heat flux tests of tungsten divertor targets under plasma heat loads expected in ITER and tokamaks”. In: *Physics of Atomic Nuclei* 79 (2016), pp. 1137–1162.

[6] PC Stangeby and AW Leonard. “Obtaining reactor-relevant divertor conditions in tokamaks”. In: *Nuclear Fusion* 51.6 (2011), p. 063001.

[7] PC Stangeby. “Basic physical processes and reduced models for plasma detachment”. In: *Plasma Physics and Controlled Fusion* 60.4 (2018), p. 044022.

[8] SI Krasheninnikov, AS Kukushkin, and AA Pshenov. “Divertor plasma detachment”. In: *Physics of Plasmas* 23.5 (2016).

[9] SI Krasheninnikov, A Yu Pigarov, and DJ Sigmar. “Plasma recombination and divertor detachment”. In: *Physics Letters A* 214.5-6 (1996), pp. 285–291.

[10] L Casali et al. “Improved core-edge compatibility using impurity seeding in the small angle slot (SAS) divertor at DIII-D”. In: *Physics of Plasmas* 27.6 (2020).

[11] A Kallenbach et al. “Impurity seeding for tokamak power exhaust: from present devices via ITER to DEMO”. In: *Plasma Physics and Controlled Fusion* 55.12 (2013), p. 124041.

[12] Arne Kallenbach et al. “Partial detachment of high power discharges in ASDEX Upgrade”. In: *Nuclear Fusion* 55.5 (2015), p. 053026.

[13] R Maingi. “Investigation of Physical Processes Limiting Plasma Density in DIII–D”. In: *APS Division of Plasma Physics Meeting Abstracts*. 1996, 5IB–03.

[14] D Silvagni et al. “Impact of divertor neutral pressure on confinement degradation of advanced tokamak scenarios at ASDEX Upgrade”. In: *Physics of Plasmas* 31.2 (2024).

[15] Weston M Stacey. “A calculation model for density limits in auxiliary heated, gas fueled tokamaks and application to DIII-D model problems”. In: *Physics of Plasmas* 8.8 (2001), pp. 3673–3688.

[16] L Casali et al. “Modelling the effect of divertor closure on detachment onset in DIII-D with the SOLPS code”. In: *Contributions to Plasma Physics* 58.6-8 (2018), pp. 725–731.

[17] L Casali, BM Covele, and HY Guo. “The effect of neutrals in the new SAS divertor at DIII-D as modelled by SOLPS”. In: *Nuclear Materials and Energy* 19 (2019), pp. 537–543.

[18] B Lipschultz et al. “Neutrals studies on alcator C-Mod”. In: *Fusion science and technology* 51.3 (2007), pp. 390–400.

[19] AL Moser et al. “Separating divertor closure effects on divertor detachment and pedestal shape in DIII-D”. In: *Physics of Plasmas* 27.3 (2020).

[20] L Casali et al. “Neutral leakage, power dissipation and pedestal fueling in open vs closed divertors”. In: *Nuclear Fusion* 60.7 (2020), p. 076011.

[21] L Casali et al. “Impurity leakage and radiative cooling in the first nitrogen and neon seeding study in the closed DIII-D SAS configuration”. In: *Nuclear Fusion* 62.2 (2022), p. 026021.

[22] R Martin. “MAST Upgrade.—Construction Status and Early Research Plans”. In: *IAEA Report* (2014).

[23] William Morris et al. “MAST upgrade divertor facility: a test bed for novel divertor solutions”. In: *IEEE transactions on plasma science* 46.5 (2018), pp. 1217–1226.

[24] D Brunner et al. “The dependence of divertor power sharing on magnetic flux balance in near double-null configurations on Alcator C-Mod”. In: *Nuclear Fusion* 58.7 (2018), p. 076010.

[25] SS Henderson et al. “Validating reduced models for detachment onset and reattachment times on MAST-U”. In: *Nuclear Materials and Energy* 41 (2024), p. 101765.

[26] V Rozhansky et al. “New B2SOLPS5. 2 transport code for H-mode regimes in tokamaks”. In: *Nuclear fusion* 49.2 (2009), p. 025007.

[27] Detlev Reiter, Martine Baelmans, and Petra Boerner. “The EIRENE and B2-EIRENE codes”. In: *Fusion science and technology* 47.2 (2005), pp. 172–186.

[28] Xavier Bonnin et al. “Presentation of the new SOLPS-ITER code package for tokamak plasma edge modelling”. In: *Plasma and Fusion Research* 11 (2016), pp. 1403102–1403102.

[29] Sven Wiesen et al. “The new SOLPS-ITER code package”. In: *Journal of nuclear materials* 463 (2015), pp. 480–484.

[30] OP Bardsley, JL Baker, and C Vincent. “Decoupled magnetic control of spherical tokamak divertors via vacuum harmonic constraints”. In: *Plasma Physics and Controlled Fusion* 66.5 (2024), p. 055006.

[31] Juan Francisco Rivero-Rodríguez et al. “Overview of fast particle experiments in the first MAST Upgrade experimental campaigns”. In: *Nuclear Fusion* 64.8 (2024), p. 086025.

[32] Lina Velarde et al. “Velocity-space analysis of fast-ion losses measured in MAST-U using a high-speed camera in the FILD detector”. In: *Plasma Physics and Controlled Fusion* 67.1 (2024), p. 015024.

[33] David Moulton et al. “Super-X and conventional divertor configurations in MAST-U ohmic L-mode; a comparison facilitated by interpretative modelling”. In: *Nuclear Fusion* 64.7 (2024), p. 076049.

[34] W Eckstein and DB Heifetz. “Data sets for hydrogen reflection and their use in neutral transport calculations”. In: *Journal of Nuclear Materials* 145 (1987), pp. 332–338.

[35] C Garcia-Rosales, W Eckstein, and J Roth. “Revised formulae for sputtering data”. In: *Journal of nuclear materials* 218.1 (1995), pp. 8–17.

[36] J Roth et al. “Flux dependence of carbon chemical erosion by deuterium ions”. In: *Nuclear fusion* 44.11 (2004), p. L21.

[37] D Moulton et al. “Using SOLPS to confirm the importance of total flux expansion in Super-X divertors”. In: *Plasma Physics and Controlled Fusion* 59.6 (2017), p. 065011.

[38] Wouter Dekeyser et al. “Plasma edge simulations including realistic wall geometry with SOLPS-ITER”. In: *Nuclear Materials and Energy* 27 (2021), p. 100999.

[39] W Fundamenski. “Parallel heat flux limits in the tokamak scrape-off layer”. In: *Plasma physics and controlled fusion* 47.11 (2005), R163.

[40] JG Clark, MD Bowden, and R Scannell. "Low temperature Thomson scattering on MAST-U". In: *Review of Scientific Instruments* 92.4 (2021).

[41] Peter J Ryan et al. "Overview of the langmuir probe system on the mega ampere spherical tokamak (MAST) upgrade". In: *Review of Scientific Instruments* 94.10 (2023).

[42] X Feng et al. "Development of an 11-channel multi wavelength imaging diagnostic for divertor plasmas in MAST Upgrade". In: *Review of Scientific Instruments* 92.6 (2021).

[43] TA Wijkamp et al. "Characterisation of detachment in the MAST-U Super-X divertor using multi-wavelength imaging of 2D atomic and molecular emission processes". In: *Nuclear Fusion* 63.5 (2023), p. 056003.

[44] *Open ADAS Initiative*. `https://www.openadas.com/`. 2004.

[45] AA Mavrin. "Radiative cooling rates for low-Z impurities in non-coronal equilibrium state". In: *Journal of Fusion Energy* 36.4 (2017), pp. 161–172.

[46] CS Pitcher et al. "An experimental investigation of chemical sputtering of carbon in a tokamak discharge". In: *Nuclear fusion* 26.12 (1986), p. 1641.

[47] GM McCracken and PC Stangeby. "The interpretation of plasma edge conditions in tokamaks". In: *Plasma Physics and Controlled Fusion* 27.12A (1985), p. 1411.

[48] Bob Kool et al. "First demonstration of Super-X divertor exhaust control for transient heat load management in compact fusion reactors". In: *arXiv preprint arXiv:2407.07784* (2024).

[49] SI Krasheninnikov and AS Kukushkin. "Physics of ultimate detachment of a tokamak divertor plasma". In: *Journal of Plasma Physics* 83.5 (2017), p. 155830501.